User Scheduling and Antenna Topology in Dense Massive MIMO Networks An Experimental Study

Wang, Cheng Ming; Wang, Qing; Gaber, Abdo; Guevara, Andrea P.; Pollin, Sofie

DOI
10.1109/TWC.2020.3001224

Publication date
2020

Document Version
Final published version

Published in
IEEE Transactions on Wireless Communications

User Scheduling and Antenna Topology in Dense Massive MIMO Networks: An Experimental Study

Cheng-Ming Chen, *Student Member, IEEE*, Qing Wang, *Member, IEEE*, Abdo Gaber, *Member, IEEE*, Andrea P. Guevara, *Student Member, IEEE*, and Sofie Pollin, *Senior Member, IEEE*

***Abstract*—A massive MIMO network can serve ten's of users simultaneously. However, in dense scenarios the users are potentially closely-spaced, potentially resulting in substantial inter-user interference. Scheduling can overcome this by selecting the users that lead to the highest combined spectral efficiency. As scheduling comes with a significant pilot overhead, an alternative strategy could minimize user correlation by distributing the antenna elements in space. In this paper, we propose a comprehensive system study including antenna topology and distribution, user scheduling and pilot overhead reduction. Our user scheduling and pilot reduction algorithms are evaluated using system level simulations relying on indoor line-of-sight channel measurements from a 64 antenna base station at 2.61GHz. To have a thorough evaluation of the proposed algorithm, we consider four different antenna topologies, including co-located and distributed placement of the base station arrays. Our evaluation shows that in a conference room with 64 densely deployed users, our proposed low complexity algorithm can improve the spectral efficiency by at least 14% compared to random user selection with the best antenna distribution strategy. Finally, our results show that by relying on channel hardening, we reduce the pilot overhead by 3.2x.**

***Index Terms*—Massive MIMO networks, dense networks, distributed antenna arrays, user scheduling, testbed measurements.**

I. Introduction

MASSIVE MIMO was proposed in 2010 as a new paradigm to meet the increasing demand for wireless capacity [2]. It utilizes large arrays of antennas that span tens to hundreds of wavelengths in space to serve more than ten users simultaneously. Using a large number of antennas increases the network spectral efficiency [3].

Manuscript received April 19, 2019; revised October 10, 2019 and March 16, 2020; accepted May 27, 2020. Date of publication June 17, 2020; date of current version September 10, 2020. This work was supported in part by the Flemish Hercules Foundation under Grant AKUL1318, in part by the EU H2020 Project ORCA under Grant 732174, and in part by the Research Foundation Flanders (FWO) Postdoctoral Fellowship under Grant 12Y0919N. This article was presented in part at the IEEE INFOCOM Workshop on Computer and Networking Experimental Research Using Testbeds (CNERT), Paris, France, April 29, 2019 [1]. The associate editor coordinating the review of this article and approving it for publication was M. Payaró. *(Corresponding author: Qing Wang.)*

Cheng-Ming Chen, Andrea P. Guevara, and Sofie Pollin are with KU Leuven, 3001 Leuven, Belgium (e-mail: cchen@esat.kuleuven.be; aguevara@esat.kuleuven.be; spollin@esat.kuleuven.be).

Qing Wang is with the Department of Software Technology, Delft University of Technology, 2628CD Delft, The Netherlands (e-mail: qing.wang@tudelft.nl).

Abdo Gaber is with National Instruments Dresden, 01099 Dresden, Germany (e-mail: abdo.gaber@ni.com).

Color versions of one or more of the figures in this article are available online at http://ieeexplore.ieee.org.

Digital Object Identifier 10.1109/TWC.2020.3001224

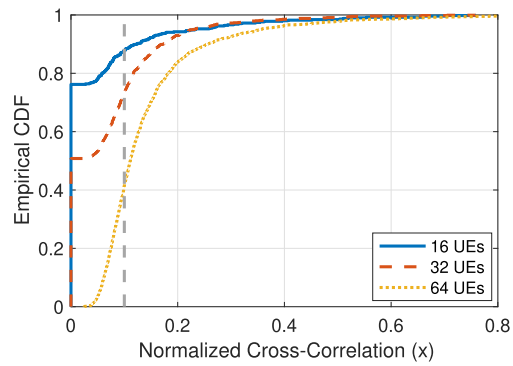

Fig. 1. The high user density leads to a significant IUC measured by normalized cross-correlation. In a dense scenario, the system performance should benefit from a proper user selection. The results are obtained from our measurements with the KU Leuven distributed massive MIMO testbed that will be detailed in Sec. VI.

A. Motivation

Traditional research on massive MIMO mainly focuses on the scenarios where user equipments (UEs) are sparsely distributed in an area. However, in many scenarios the UEs could be closely-spaced and thus experience similar channel fading patterns, *degrading the performance of traditional massive MIMO technologies due to the high IUC* [4]–[6]. The probability of having closely-spaced UEs is non-negligible, especially in indoor small cell environments [5]. To illustrate the above degradation in a real situation, below we give an example with the line-of-sight (LoS) channel measured in our department building (the measurement setup is presented in Sec. VIII-A). In this example, within the same space, the UE density increases accordingly with the number of UEs. The uplink channel correlations for such dense scenarios are analyzed in Fig. 1. Evidently, the correlation in scenarios with 64 UEs is much higher than that with fewer UEs. For instance, more than 60% of the IUC is above 0.1 in the scenario with 64 UEs, while it is only 15% and 25% in the scenarios with 16 and 32 UEs, respectively. Note that with an IUC of 0.1 between two UEs, the achieved two-user signal-to-interference ratio (SIR) will be limited to about 20 dB for each UE if their information is decoded at the base station (BS) with a simple maximum ratio combining.[1] Moreover, the traditional method of collecting CSI introduces a significant pilot overhead when there are many UEs because

[1]Under the condition that both the inter-user-interference from another nearby user and the desired signal are equal in power.

the required time is proportional to the number of UEs. Therefore, an economical design of pilot overhead to select K out of S UEs is necessary. It impacts not only the efficiency of data transmission, but also the usability in a high dynamic scenario. Furthermore, a low complexity scheduling algorithm reduces the latency for choosing the most suitable group of users. In the end, the performance will be a trade-off between spectral efficiency and user fairness.

B. Challenges

In dense indoor scenarios, there are mainly two challenges that we should solve to achieve realistic user scheduling.

Challenge 1: precise characterization of massive MIMO channels. A simple one-ring model is widely used in outdoor scenarios to characterize massive MIMO channels [3]. It models a simple scenario where a BS is surrounded by a limited number of scatterers. However, from real outdoor measurements, especially in the non-line-of-sight (NLoS) scenarios [7], [8], the angular information is very complicated as the impinging signal and reflectors to the array elements are from multiple randomly positioned scatterers. In indoor, even in LoS scenarios when there are many reflectors in the environment, the one-ring model is insufficient for the system evaluation. To date, no comprehensive model can precisely characterize the channel of large-scale antenna arrays. The per link path from each UEs to each element of the array is impacted by the antenna gain pattern. The different embedded antenna gains can impact significantly the IUC.

Challenge 2: practical user scheduling in indoor dense massive MIMO networks. When users are closely-spaced, a single BS might not be able to separate the users as for instance their angular information might be shared. Distributed antenna topologies could help to serve closely-spaced UEs better, at the cost of power imbalances caused by different path-losses between the UEs and the distributed array elements. In dense massive MIMO networks, a better strategy could be used to schedule the UEs by taking into account the IUC and thus improve the UE separation. Furthermore, most of the state of the art works have analyzed the channel after normalizing all received powers. It is reasonable when power control is applied and when the amplification gain can compensate both the large scale fading and the shadowing. However, in reality the headroom of power control is not sufficient to compensate the gap completely.

C. Contributions

In this work, we study the impact of user scheduling and antenna topologies in dense massive MIMO networks. We propose two lightweight heuristic scheduling algorithms that can alleviate the IUCs in dense networks. Different from the state of the art, our algorithms do not rely on normalized channels. We evaluate the proposed heuristic algorithms under four different antenna topologies, revealing how the positions of the BS and the UEs are related. We also analyze the impact of pilot overhead for the proposed heuristics, and show how the pilot overhead can be reduced significantly by relying on channel hardening. We summarize our contributions as below.

Contribution 1: lightweight and practical scheduling algorithms. We first formulate the problem of selecting the proper UEs to serve in an indoor dense massive MIMO networks. We need to collect the channel state information (CSI) from all the networked UEs, which brings lots of overhead especially in dynamic scenarios. To alleviate the overhead, we design a novel pilot overhead reduction method. Next, to improve the spectral efficiency, we propose two heuristic scheduling algorithms that can perform almost as good as a complicated near-optimal method, while our heuristic algorithms can avoid complex matrix inversion. Further, we embed a priority-based method into the above heuristic algorithms to improve user fairness. Together with the reduced pilot overhead, our heuristic algorithms have the potential to work well in dynamic environments. In addition, we investigate the impact of power control on the performance of the whole network. *(Sec. III, Sec. IV, and Sec. V)*

Contribution 2: testbed development and precise channel characterization. We improve our first KU Leuven massive MIMO testbed primarily. By applying 10m optical fibers to link the main computation engine with the remote radio heads (RRHs), we can distribute our 64 BS antennas from one co-located array to two sub-arrays. We also analyse the extra time delay introduced by the optical cables. This new feature of our testbed allows us to study in practice the impact of different antenna topologies on the network performance. To characterize indoor massive MIMO channels precisely, we measure the channels in an indoor conference room with 64 UEs, under four different co-located/distributed antenna topologies. The measured channel has been made open for our massive MIMO community [9]. *(Sec. VI and Sec. VII)*

Contribution 3: evaluation. We evaluate our proposed lightweight heuristic algorithms under four different antenna topologies, revealing how BS location, antenna array orientation and UEs are related. We compare the performance of our heuristic algorithms with two benchmarks. Our results show that the proposed algorithms can perform similar to the benchmark capacity-based 'sub-optimal' method, but our algorithms have much lower complexity. Furthermore, the evaluation results show that our designed priority selection method can achieve user fairness of more than 0.5 for all the scenarios we consider. *(Sec. VIII)*

The notations in this paper are as below. Uppercase boldface $\mathbf{A}$ denotes a matrix while lowercase boldface $\mathbf{a}$ indicates a column vector. Superscripts T, H, -1 and $*$ mean the transpose, Hermitian, inverse operation of a matrix and complex conjugate operation, respectively. Moreover, $\mathbb{E}(\cdot)$, $\|\mathbf{A}\|$ and $tr(\cdot)$ are the expectation operation, ℓ^2-norm of the matrix $\mathbf{A}$ and trace operation, respectively. $\arg\{\cdot\}$ represents argument of a function. $\setminus\{A\}$ stands for excluding element A from a set and the cardinality of the set A is represented as $|A|$. Finally, $[\cdot]_{nn}$ denotes the n_{th} diagonal element and $\mathbf{A} = diag(a_1, \ldots, a_n)$ stands for a diagonal matrix $\mathbf{A}$ with its elements.

II. Related Work

Although scheduling has been investigated for several decades, there are still opportunities to improve the

performance of scheduling, especially in the generation of wireless communication networks that leverage high-frequency band RF to primarily increase the network data rate. For example, scheduling is a hot topic in IEEE 802.11ax, demonstrated by a recent research published on a top-venue [10]. In this section, we review the work most related to our proposed lightweight heuristic for dense indoor massive MIMO networks.

Various channel metrics and their impact on user scheduling have been analyzed. The effect of channel correlation is studied in [11], where the authors design a new scheduler to enhance the spectral efficiency per user by avoiding serving users with highly correlated channels in the same time slot. An extended version is published in [12], where power control and spectral fairness per user are considered. A different user scheduling approach is presented in [13]. The idea is to group UEs by the largest chordal distance. This work builds a comprehensive relationship for all the UEs, which is quite computationally demanding and impractical in a dynamic environment. In [14], similarly, multiple UEs are grouped based on the dominant directions and selected according to a channel quality indicator. A similar approach is considered in [15], [16] but applied to ultra-dense scenarios. There, the system groups UEs according to the same channel covariance eigenspace spanning [15] or angle-of-arrival [16], which are obtained after a pre-beamforming matrix. Compared to the above research, we consider the power control and user fairness from the beginning in the design of our heuristic algorithms. The above UEs grouping methods rely on perfectly known CSI and neglect the pilot overhead collection that is needed to obtain sufficient channel information to achieve user grouping or scheduling. Unlike them that introduce complexity collaborations among the UEs and not practical in dynamic networks, our algorithm selects the most suitable UEs to serve. Enabled by the reduction of pilot overhead and a simple design on the scheduling, our algorithm is lightweight and could work well in dynamic networks.

Another aspect that distinguishes our research from state of the art is that we rely on the channel measured with the real testbed. However, for state of the art, the channel statistics are mostly derived from models. In [17], a closed-form expression for SINR is derived based on the channel statistics from the one-ring channel model. Then, the location-dependent user selection problem is solved by relying on a standard search algorithm. However, a simple closed-form is not reachable in a real propagation environment. Another point that should be considered is the power imbalance or gain normalization among these UEs. As for a more realistic massive MIMO channel model, the extended COST 2100 model [18] is proposed and adjusted from a massive MIMO channel measurement campaign. However, the extension and some parameters are obtained from a virtual linear array. The mutual coupling, which causes gain variation [19] among the finite antennas, is not considered in a virtual antenna array. Moreover, it is not realistically captured in the virtual array, where it impacts the cluster visibility region derived from the angular transform algorithms [20]. The aforementioned state of the art relies either on simulations or virtual arrays. There are no experiments in these works.

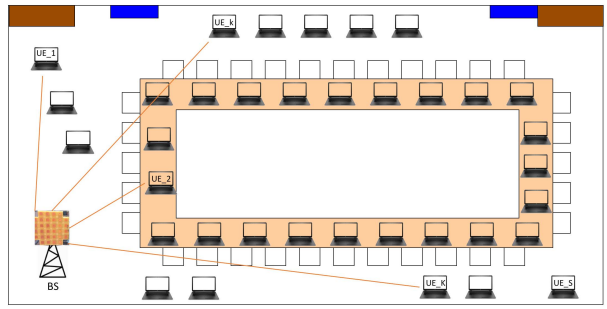

Fig. 2. The problem of user scheduling in a dense indoor massive MIMO system. The goal is to select K UEs among a total of S UEs. While maximizing the spectral efficiency, the user fairness is another crucial factor to be considered.

III. System Description

We consider a dense network with one BS and S UEs, as shown in Fig. 2. The BS is equipped with M antennas while each UE has a single antenna. Let $\mathcal{S} \triangleq \{1, \ldots, S\}$ represent the set of all the UEs. Under the configuration of a scheduling algorithm, at each coherence time τ_c the BS selects K out of S UEs for multi-user MIMO data transmission. Note that in the time division duplexing (TDD) based system, it is normally assumed that the coherence time is a summation of the time slots for transmitting uplink pilot τ_{up}, uplink data τ_{ud}, downlink pilot τ_{dp} and downlink data τ_{dd}. The BS needs to collect the CSI of UEs in order to schedule them efficiently.

Channel model: The complete multi-user massive MIMO orthogonal frequency division multiplexing (OFDM) system requires CSI in the three dimensions spanning the number of users S, the number of antennas M and the number of subcarriers Q. At the BS, after the fast fourier transform (FFT) operation, the least square estimate of the CSI $\mathbf{h}_{k,q} \in \mathbb{C}^M$ using the OFDM pilots can be obtained for the kth UE at the qth subcarrier as [21]

$$\mathbf{h}_{k,q} = \beta_k^{\frac{1}{2}} \mathbf{g}_{k,q} + \mathbf{n}, \tag{1}$$

where β_k denotes the frequency-flat large scale fading and $\mathbf{n}$ is the additive white Gaussian noise (AWGN) that is independent and identically distributed (i.i.d.) $\mathbf{n} \sim \mathcal{N}_{\mathbb{C}}(\mathbf{0}_M, \sigma_{UL}^2 \mathbf{I}_M)$. It is to be kept in mind that $-\frac{Q-1}{2} \leq q \leq \frac{Q-1}{2}$, where Q is the number of useful subcarriers.

Uplink spectral efficiency: The analysis of the spectral efficiency provides us key information for the design of the user scheduling algorithms.

The user scheduling algorithm is to select a set of active UEs to serve, denoted by $\mathcal{S}_{ac}$, given that $\mathcal{S}_{ac} \subset \mathcal{S}$ and $|\mathcal{S}_{ac}| = K$. We will explain the user selection algorithm in the next section. Herein, the per subcarrier uplink received signal at the BS from the selected K active UEs can be represented as:

$$\mathbf{y}_q = \sum_{k \in \mathcal{S}_{ac}} \mathbf{h}_{k,q} s_{k,q} + \mathbf{n}, \tag{2}$$

where $\mathbf{y}_q \in \mathbb{C}^M$. The uplink signal from UE k is denoted by $s_{k,q} \in \mathbb{C}$ and has power $p_{k,q} = \mathbb{E}\{|s_{k,q}|^2\}$. The BS calculates a spatial discrimination vector $\mathbf{v}_{k,q}$ to decode the data stream

on subcarrier q from UE k. The minimum mean square error (MMSE) combiner maximizes the signal-to-interference-and-noise ratio (SINR) and is represented as [3]

$$\mathbf{v}_{k,q} = p_{k,q}\left(\sum_{i\in\mathcal{S}_{ac}} p_{i,q}(\mathbf{h}_{i,q}\mathbf{h}_{i,q}^H) + \sigma_{UL}^2\mathbf{I}_M\right)^{-1}\mathbf{h}_{k,q}. \quad (3)$$

If we define a diagonal matrix $\mathbf{P} = \mathrm{diag}(p_{1,q},\ldots,p_{K,q})$, the combining vectors for all UEs after some matrix transformation, can be collected and represented in a compact form,

$$\mathbf{V}_q = [\mathbf{v}_{1,q}\ldots\mathbf{v}_{K,q}] = \mathbf{H}_q\left(\mathbf{H}_q^H\mathbf{H}_q + \sigma_{UL}^2\mathbf{P}^{-1}\right)^{-1}, \quad (4)$$

where the channel matrix $\mathbf{H}_q = [\mathbf{h}_{1,q}\ldots\mathbf{h}_{K,q}]$. The resulting SINR per subcarrier is therefore [3], [22]

$$\mathrm{SINR}_{k,q}^{\mathrm{UL}} = \frac{p_{k,q}}{\sigma_{UL}^2\left[\left(\mathbf{H}_q^H\mathbf{H}_q + \sigma_{UL}^2\mathbf{P}^{-1}\right)^{-1}\right]_{kk}} - 1. \quad (5)$$

The average uplink spectral efficiency per UE k is defined as

$$\mathrm{SE}_k = \frac{\tau_{ud}}{\tau_c}\mathbb{E}\left(\log_2(1+\mathrm{SINR}_{k,q}^{\mathrm{UL}})\right), \quad (6)$$

where the sample mean is taken over subcarriers q. All expectations are with respect to the channel realizations. The pre-log factor will be explained in detail Sec. VIII.

From Eq. (5) and [19] and [23], we observe that a high channel gain variance in the selected UE set has a negative impact on user fairness. The average channel gain per UE is an important information and can be represented as

$$\bar{\mathbf{h}}_k = M\beta_k = \mathbb{E}\{\|\mathbf{h}_{k,q}\|^2\}. \quad (7)$$

User fairness: The uplink CSI provides us sufficient information to reach the maximum system throughput. However, user fairness should also be highlighted while designing a user scheduling strategy. The long term fairness among all users in the network can be evaluated via the Jain's Fairness Index (JFI) [24]. It is defined as

$$\mathcal{F} = \frac{(\sum_{k\in\mathcal{S}}\omega_k\mathrm{SE}_k)^2}{S\sum_{k\in S}(\omega_k\mathrm{SE}_k)^2}, \quad (8)$$

where ω_k is the probability that the k_{th} UE being selected for service. Note that $\sum_{k\in\mathcal{S}}\omega_k = 1$ and $\sum_{k\in\mathcal{S}_{ac}}\omega_k = \frac{K}{S}$.

IV. Proposed Heuristic Scheduling Algorithm

Our objective is to maximize the network spectral efficiency:

$$\max\sum_{k\in\mathcal{S}}\mathrm{SE}_k. \quad (9)$$

From the system performance perspective, selecting a subset of UEs with the lowest IUC seems preferable. However, the selection process is complex according to Eq. (4). The combining matrix requires a matrix inversion which depends on the UEs in the already selected set. Moreover, finding the optimal user scheduling typically requires an exhaustive performance evaluation of all combinations, instead of a greedy search, incurring prohibitively high computation cost even with a moderate number of UEs. Therefore, we apply the main concept in a sub-optimal greedy user scheduling approach [25], [26], but with a modified per iteration UE selection method.

In this section, we present the proposed Gram-matrix based heuristic scheduling algorithm. The selection algorithm is based on a sufficiently channel over subcarriers if OFDM is assumed. When OFDMA is used, and different users can be scheduled for each resource block, we assume the algorithm is carried out independently for each resource block. As the user scheduling is done assuming a flat channel, we omit the subcarrier index q in this section, and will generalize this again later when discussing the pilot overhead. To reduce the overhead on the uplink CSI collection, we further design a pilot overhead reduction method based on the concept of channel hardening in massive MIMO networks. We also take user fairness into account in designing the heuristic algorithm.

Two variations of the proposed heuristic algorithm are designed for the IUCs calculations and user selection. One is referred as the Min-Max Gram-Matrix (MinMaxGramM) based heuristic. The other one is the Summation of Normalized Gram-Matrix (MinSNGramM) based heuristic.

A. MinMaxGramM: Min-Max Gram-Matrix Based heuristic

In our algorithm, we select the K UEs one by one in a greedy search. Each time when we select a new UE, we make sure that the IUC it introduces to the system is minimized according to a certain criterion. The first proposed MinMaxGramM heuristic algorithm is described in Algorithm 1. The four main steps are introduced as follows.

Step 1: Initialization

In each scheduled resource block, we first select a first UE in the initialization. The UE can be the one that has the highest spectral efficiency, or the one has the least IUC with other UEs. In this work, we want to ensure the fairness among the UEs. Therefore, in the initialization, we select the UE with the lowest historical spectral efficiency. That is, we select an UE k_1 that satisfies

$$k_1 = \arg\min_{k\in\mathcal{S}}\mathrm{SE}_k \quad (10)$$

where SE_k is given in (6). Except for the selection of a primary UE, we also initialize an empty set $\mathcal{D}$ to store the IUC. These operations are given in Lines 1 to 3 of Algorithm 1.

Step 2: Calculate the IUCs introduced by each new possible UE

Note that when we select the ith UE, we evaluate the IUCs introduced by all the UEs that have not been selected for service in the current scheduled resource block. We approximate IUCs between the new UE under examination to all the previous $i-1$ UEs that have been selected. As shown in Line 6 of Algorithm 1, we will consider multiple user selection methods.

The key question answered in this section is: *How to approximate the IUCs efficiently?* We have derived some insights in our previous study of the IUC calculation of a two-UE scenario [19]. Two vital findings can be considered when determining the ith UE in every iteration. This can be observed by the Gram-matrix $\mathbf{C}_i$ associated with $\mathbf{H}_i = [\mathbf{h}_{k_1}\ldots\mathbf{h}_i]$ (Note that at iteration i, a number of $i-1$

Algorithm 1 Outline of the Greedy User Paradigm

Input: $\{\text{SE}\} = \{\text{SE}_1 \ldots \text{SE}_S\}$, $\mathcal{S} = \{1, \ldots, S\}$, $\mathcal{S}_{ac} = \emptyset$, K, K_{pri}
Output: $\mathcal{S}_{ac}$, $\{\text{SE}\}$
1: **Initialization** select k_1 from Eq. (10), $\mathcal{S}_{ac} = \{k_1\}$, $\mathcal{S} = \mathcal{S} \backslash \{k_1\}$, $\mathbf{H}_1 = \mathbf{h}_{k_1}$, $i = 2$
2: **while** $|\mathcal{S}_{ac}| < K$ **do**
3: Initialize $\mathcal{D} = \emptyset$
4: **for** `all` $k \in \mathcal{S}$ **do**
5: $\mathbf{H}_i = [\mathbf{H}_{i-1}\, \mathbf{h}_k]$
6: $\delta_i = \text{US}_{\text{method}}(\mathbf{H}_i)$, $\mathcal{D} = \mathcal{D} \cup \{\delta_i\}$
7: **end for**
8: $s_i = \text{US}_{\text{selection}}(\mathcal{D}, \text{SE}, K_{pri})$
9: $\mathcal{S}_{ac} = \mathcal{S}_{ac} \cup \{s_i\}$, $\mathcal{S} = \mathcal{S} \backslash \{s_i\}$
10: $\mathbf{H}_i = [\mathbf{H}_{i-1}\, \mathbf{h}_{s_i}]$
11: $i = i + 1$
12: **end while**
13: update $\{\text{SE}\}$

UEs have been decided):

$$\mathbf{C}_i = \mathbf{H}_i^H \mathbf{H}_i = \begin{bmatrix} \mathbf{C}_{i-1} & \mathbf{c}_i \\ \mathbf{c}_i^H & c_{i,i} \end{bmatrix}. \tag{11}$$

When the ith UE is evaluated, $i-1$ new IUCs, denoted by the vector $\mathbf{c}_i$, are generated. Based on this, the SINR determining the SE of the link will be decided. There are two main factors affecting the SINR, the first being the channel gain in the nominator, and the second being the interference in the denominator. When we compare UEs, we see that the first reason for the SINR imbalance comes from the gain imbalance between the UEs, which can be interpreted from the gain difference among the diagonal terms. The second factor is the IUC contributed from the non-diagonal upper triangular terms. Heuristically, we can first limit the power difference between the candidate UE and the selected UEs, then minimize their IUC. However, in a real scenario, when the UEs share similar power, they might be closely located with a high probability. While applying this gain based greedy selection, we might miss the best, most uncorrelated, candidate. Thus, in our heuristic, no power pre-selection is applied and the focus is on limiting the power of IUCs.

In MinMaxGramM, at each iteration i, we normalize the new generated IUC $\mathbf{c}_i$ with respect to $c_{i,i}$. The target is to find a candidate UE to minimize the maximum value in this set (Line 6 in Algorithm 1):

$$\begin{aligned} \delta_i &= \max\left(\hat{\mathbf{c}}_i\right) \\ &= \max\left((c_{i,i})^{-1} p_i^{-1/2} \left[p_1^{1/2} |c_{1,i}|, \ldots, p_{i-1}^{1/2} |c_{i-1,i}| \right]^T \right), \end{aligned} \tag{12}$$

where p_i is the transmit power of UE i. Note that each element of $\hat{\mathbf{c}}_i$ is a scaled correlation between the jth and i^{th} UE and can be interpreted as

$$\hat{c}_{j,i} = \left(\frac{p_j}{p_i}\right)^{1/2} \frac{\|\mathbf{h}_j\|}{\|\mathbf{h}_i\|} \cos(\theta_{\mathbf{h}_j \mathbf{h}_i}),\ 1 \le j \le i-1, \tag{13}$$

where $0 \le \cos(\theta_{\mathbf{h}_i \mathbf{h}_j}) \le 1$ represents the normalized correlation between the two channel vectors. Interesting, there is an antagonism between $\|\mathbf{h}_i\|$ and $|c_{j,i}|$. On the one hand, we hope to include a UE that contributes more to the capacity. Therefore, a high power in $\|\mathbf{h}_i\|$ is preferred. On the other hand, the smallest correlation is also a big desire, the lower $\|\mathbf{h}_i\|$ seems to give us lower $|c_{j,i}|$.

Step 3: Select the ith UE that introduces minimized IUCs, with tradeoff on fairness

The candidate s_i is determined based on a certain criterion. The target is to find the best UE in the ith iteration, which introduces the minimized IUCs. To improve the user fairness, in our heuristic we first sort the set $\mathcal{D}$ from the lowest to highest. Then, we select from the set $\mathcal{D}$ a number of K_{pri} UEs that introduce the lowest IUCs. Among these K_{pri} UEs, we select the UE that has the least historical spectral efficiency. The above operations are denoted by the function $\text{US}_{\text{selection}}$ in Algorithm 1 (Line 8).

Step 4: Iteration

Next, we update the final set, as shown in Line 9-11 of Algorithm 1. Finally, the whole scheduling process is finished when all the K UEs are found. Afterwards, the new averaged spectral efficiency per UE is updated for next scheduling, as shown in Line 13 of Algorithm 1. Note that there is no special requirement to set the initial values or threshold in different scenarios such as the different deployment of the antennas. Our proposed algorithm can be applied to any scenarios with different antenna topologies.

B. MinSNGramM: Minimized Summation of Normalized Gram-Matrix Based Heuristic

We also propose another criterion to approximate the IUC introduced by a new UE. Instead of minimizing the maximal IUC in *Step 3*, we minimize the normalized Gram-Matrix. We call this heuristic MinSNGramM. That is, the aim is to minimize the summation of the normalized IUCs

$$\delta_i = \sum_{j=1}^{i-1} \hat{c}_{j,i} = \sum_{j=1}^{i-1} \frac{p_j^{1/2} |c_{j,i}|}{(p_i c_{j,j} c_{i,i})^{1/2}}. \tag{14}$$

Each $\hat{c}_{j,i}$ can be interpreted as

$$\hat{c}_{j,i} = \left(\frac{p_j}{p_i}\right)^{1/2} \cos(\theta_{\mathbf{h}_j \mathbf{h}_i}), \tag{15}$$

where all the power in the individual channel vector is excluded as compared to Eq. (13). In Fig. 1, the correlation curve is drawn with this expression.

C. Pilot Overhead Discussion and Reduction

The pilot overhead reduces the time available for data transmission and degrades the spectral efficiency. For data reception, full CSI is needed which means that we should have for each user or data stream, a pilot in each time and bandwidth coherence block. When the number of users is large, and when the bandwidth of the system is significantly larger than the coherence bandwidth, this means many pilots need to be scheduling in a coherence time, reducing the spectral efficiency. Ideally, it should be possible to require full CSI only for the K scheduled users, and schedule the

users from only partial CSI obtained for all the S users in the system.

The principle behind the proposed pilot overhead reduction method comes from the concept of channel hardening in massive MIMO. Here, we assume that the user scheduling criterion does not require full CSI, especially to approximate the IUCs calculation. Such partial CSI will not be able to determine the full correlation or gain imbalance across users, but significantly reduces the pilot cost. This means in practice that we can utilize only one OFDM symbol to obtain the CSI from all S UEs. That is to say, if we could do user scheduling on any $\mathbf{h}_{k,q}$, for a random q, up to Q pilots could be scheduled into a single OFDM symbol. In most systems, $S \gg K$ so this means that at maximum one OFDM symbol is needed.

However, we have to send pilot symbols from the selected K UEs for data detection. Therefore, the overall pilot overhead is only proportional to $K+1$. In this paper, we verify this IUC calculation tolerance only in the measured LoS channel.

D. Uplink Power Control

The BS normally has a limited analog-to-digital converter (ADC) headroom with low resolution. To pave the way for it, we design a simple uplink power control method and apply it before the scheduling algorithm. Not that most user selection algorithms rely on normalized channels, while ours is not. However, the power control we discuss in this subsection can be seen as a partial channel normalization, to make sure the gain imbalances in the system are acceptable. The UEs transmit different power according to their distance to the BS. When signals arrive at the BS, the maximum power received at the BS can be at most δ_p dB bigger than the minimum received power, to limit the gain imbalance. By assuming that the farthest UE k transmits a maximum power p_k equal to $P_{\max} > 0\,\text{dBm}$, the power of the users close to the base station is reduced. The resulting transmit power of each UE is closely related to the large scale-fading β_k and can be defined as:

$$p_k = \begin{cases} P_{max}, & \beta_k - \delta_p < \beta_{k,min} \\ P_{max} - (\beta_k + \delta_p) + \beta_{k,min}, & \beta_k - \delta_p \geq \beta_{k,min} \end{cases}, \tag{16}$$

where all expressions in the equation are in dB scale and $\beta_{k,min}$ is the link gain of the farthest UE in a scenario. It is worthwhile to mention two points. First, the power control here is not treated differently for the distributed-array cases. Second, from (5), we can expect that the output of the user scheduling algorithm will be adapted to the power redistribution and will improve the performance of user fairness.

V. Complexity Analysis

In this section, we analyze the joint computational complexity of the user selection and MIMO MMSE data detection algorithms. Both require the frequent computation of complex operations such as Gram-matrix and matrix inversion. *We use another two algorithms for comparisons: capacity based scheduling and random scheduling. The details of these two scheduling algorithms can be found in Sec. VIII.* Depending on the algorithm, the number of times we should compute these complex operations varies significantly, as quantified below. The MIMO combining vector algorithm has been included in the analysis for a fair comparison. As in the end, even the Random selection method requires MIMO detection, while the other methods can reuse computations performed during the user selection procedure.

For the Random scheduling, the computations are only for the MIMO detector, and this requires the computation of one Gram-matrix and one matrix inverse. However, for the greedy user selection algorithms it is necessary to compute the Gram-matrix or matrix inverse multiple times, for increasing matrix dimensions until K users have been selected. As for the Capacity based scheduling, it further requires to compute the same amount of times for matrix inversion.

The dominant computation for user scheduling is the Gram-matrix computation. The size of the matrix and hence the number of elements is proportional to the total number of users in the network S and the number of users K that will be selected. The elements of the Gram-matrix should be calculated in each greedy selection loop. [2] For Random scheduling, only one Gram-matrix should be computed with $K \times K$ elements. It is worth mentioning that the Gram-matrix has a symmetric structure. Hence, we only need to calculate the upper triangular elements. The calculation of each element requires M^2 complex multiplications. An example for typical system dimensions is presented in Table I.

The computation of matrix inversion can be referenced from the Lemma B.2 of [3]. For a $K \times K$ matrix, the number of complex multiplication is $\frac{K^3+2K}{3}$. The vast number of matrix inversions is required in the Capacity based scheduling, and cannot be pre-calculated, since the recalculation is necessary for a different Gram-matrix. On the contrary, it is required to calculate only one Gram-matrix inversion for the Random and GramM based scheduling algorithms in the second stage. The overall complexity, excluding Gram-matrix calculation, is tabulated in Table II. The computational complexity of the proposed method is around 0.5% of the Capacity based scheduling, which is a significant complexity reduction.

VI. Distributed Massive MIMO Testbed Design

Most of the state-of-the-art measurement campaigns and testbed designs for massive MIMO networks focus on co-located antenna array topology [23], [28]–[30]. Our massive MIMO testbed in KU Leuven is designed for distributed massive MIMO research [4], [31]. The main components of our testbed and their functionalities are described in Table III.

Fig. 3a presents the 64 patch antennas and how they are distributed into two homogeneous rectangular arrays. Each antenna array is controlled by a subsystem of 16 National Instruments universal software radio peripherals (USRPs) that supports 32 RRHs. The two sub-systems are connected to a MIMO processor through two 10-meter optical fibers, as shown in Fig. 3b. The MIMO processor is used for the back-haul In-phase and quadrature (I/Q)

[2] If the K is large, it is more efficient to do the pre-stored meaning that we compute all combinations exhaustively and store it in a look up table (LUT). For the pre-stored way, we pre-calculate $S \times S$ elements.

TABLE I

COMPUTATIONAL COMPLEXITY REQUIRED FOR GRAM-MATRIX CALCULATION. A NUMERICAL EXAMPLE FOR $K = 16$, $M = 64$ AND $S = 64$ IS GIVEN. FOR THE PROPOSED AND THE CAPACITY BASED GREEDY SEARCH METHODS, WE CAN COMPUTE THE GRAM-MATRIX EACH TIME *per greedy loop* OR DETERMINE A GRAM-MATRIX *pre-stored* IN A LUT. WHEN K IS LARGE, AS IN OUR CASE, IT IS OPTIMAL TO RELY ON THE *pre-stored* LUT

Gram-matrix computation requirement	Number of Complex Multiplications	Numerical example
Computation *per greedy loop* for K iterations	$\left[\sum_{k=1}^{K} k(S-k+1)\right] \times M^2$	$0.3E9$
Pre-stored LUT	$\left[\sum_{k=1}^{S} k\right] \times M^2$	$8.5E6$
Once for K randomly selected users	$\left[\sum_{k=1}^{K} k\right] \times M^2$	$0.56E6$

TABLE II

COMPUTATIONAL COMPLEXITY FOR THE MATRIX INVERSE WHICH IS NEEDED AT LEAST ONCE TO DETERMINE THE COMBINING VECTORS. A NUMERICAL EXAMPLE WHEN $K = 16$, $M = 64$, $S = 64$ IS GIVEN

Matrix inverse computation requirement	Number of Complex Multiplications	Numerical example
Once for GramM or Random scheduling	$\frac{K^3+2K}{3}$	$1.4E3$
For K iterations for capacity based scheduling	$\sum_{k=1}^{K}\left[\frac{K^3+2K}{3} \times (S-k+1)\right]$	$0.3E6$

TABLE III

THE MAIN COMPONENTS OF OUR MASSIVE MIMO TESTBED. THESE COMPONENTS ARE PROVIDED BY NATIONAL INSTRUMENTS. AN OFFICIAL GUIDE FROM NATIONAL INSTRUMENTS FOR MIMO PROTOTYPING IS AVAILABLE IN [27]

Equipment	Quantity	Function
USRP 2942R	32	Remote Radio Heads, each controls two data streams through two patch antennas.
PXIe-8374	32	Communication between data distributors and RRHs.
PXIe-8384	4	Communication between main controller and data distributors of subsystems.
PXIe-7976	2	MIMO processing operations such as precoding and equalization, as well as channel estimation.
PXIe-6674T	1	Timing and Synchronization.

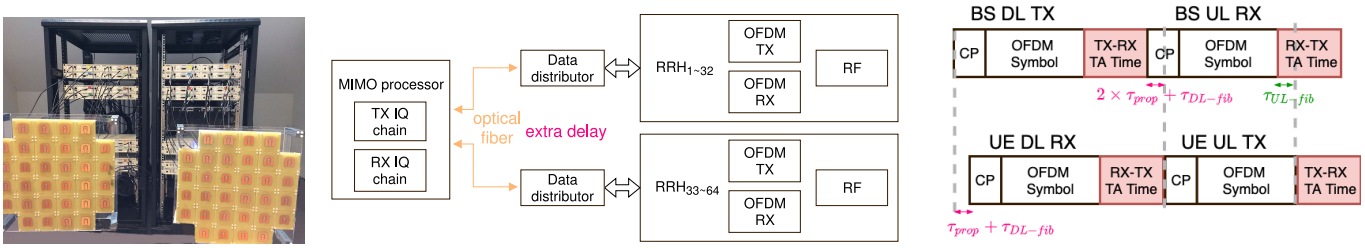

(a) The two distributable 32-antenna arrays in our testbed.

(b) System block diagram to demonstrate the extra delay caused by optical fibers.

(c) The analysis of how extra delay can be handeled by uplink cyclic prefix and RX-TX turnaround time at BS.

Fig. 3. Our designed distributed massive MIMO testbed. It consists of two distributable 32-antenna arrays. Two sub-systems, each with 32 RRHs, are connected by two 10-meter optical fibers to a central MIMO processing unit.

centralized processing. [3] With the use of optical fibers, some extra fiber delays, i.e., downlink and uplink fiber delays (denoted as τ_{DL-fib} and τ_{UL-fib}, respectively), are introduced, compared to the short Multisystem eXtension Interface (MXI) copper cable assembled in the system with co-located antenna arrays [28]. The propagation speed in fiber cable is approximately 80% of that in copper cable. In our testbed, the delay difference is around 7 OFDM samples. Therefore, distributing the antenna arrays requires extra design and testing of the testbed.

[3]Note that one of the sub-systems is bundled to the MIMO processor in the same rack. Therefore, the maximum separation of the two sub-systems is 10m instead of 20m.

How to mitigate the above extra delay? In our TDD based massive MIMO system, we analyze how the tested can tolerate the extra delay. We leverage the exemplary frame structure shown in Fig. 3c for illustration. Keep in mind that the frame timing is managed by the BS. At the beginning of each frame, in the downlink, the OFDM symbol reaches the UE with a wireless propagation delay denoted by τ_{prop}, plus the downlink fiber delay τ_{DL-fib}. Then, the UE starts a TX OFDM symbol after an RX-TX turnaround time counter. For the BS, it starts the receiving mode by assuming that the uplink symbol arrives at itself after a TX-RX turnaround time. As shown by the flow presented in Fig. 3c, the two times of τ_{prop} and the τ_{DL-fib} can be covered by the cyclic prefix in the uplink symbol. It can also be compensated by shortening

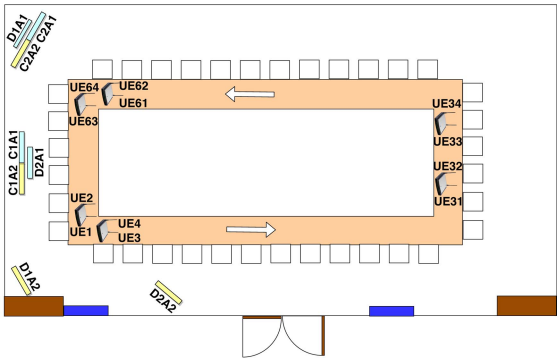

(a) Block diagram of the measurement setup.

(b) Snapshot of the measurement setup.

Fig. 4. Indoor channel characterization conducted in a meeting room with four different antenna array topologies: C1, C2, D1, and D2 (*C: co-located scenarios; D: distributed scenarios).*

the TX-RX turnaround time in the BS. The uplink I/Q samples reach the MIMO processor in the BS with a delay of τ_{UL-fib}, which can be covered by a proper design of the RX-TX turnaround time. Note that for a distributed massive MIMO system, other design perspectives have to be considered. For instance, the TDD reciprocity calibration algorithm of a distributed massive MIMO has been improved in [31]; it reduces the downlink precoded inter-user interference.

VII. Indoor Channel Characterization With Testbed Measurements

To evaluate the proposed scheduling algorithm with real setups as well as to study the impact of antenna topologies on the system performance, we perform channel characterizations with our designed testbed. Our channel characterizations with testbed measurements are conducted in a conference room with size of 13.2 m $\times$ 7.1 m, as shown in Fig. 4. We use two distributed antenna arrays, *labeled as A1 and A2 for array one and array two, respectively*. Each array is equipped with 32 patch antennas. A combination of four different antenna topologies at the BS are studied:

- *Antenna topology C1:* stands for the topology Co-located 1, where the two antenna arrays A1 and A2 are located in the front of the meeting room.
- *Antenna topology C2:* stands for the scenario Co-located 2, where the two antenna arrays A1 and A2, next to each other, are set aside of the meeting room with 30° clockwise rotation from the front side wall.
- *Antenna topology D1:* stands for the scenario Distributed 1, where the two antenna arrays A1 and A2 are set in both corners of the front of the room. They are also with 30° rotation, one clockwise and the other counterclockwise from the wall.
- *Antenna topology D2:* represents the scenario Distributed 2, where the antenna array A1 is located in the front of the room, and A2 is set in the side with 45° clockwise rotation. The inter-array distance of the two antenna arrays is 7 m.

The environment is kept static during the measurements. Nevertheless, each measurement on the UE side was collected one by one by moving two USRPs, where each USRP act as two UEs. Every two UEs on the same USRP have a distance of around two wavelengths. As indicated in Fig. 4a, we deploy

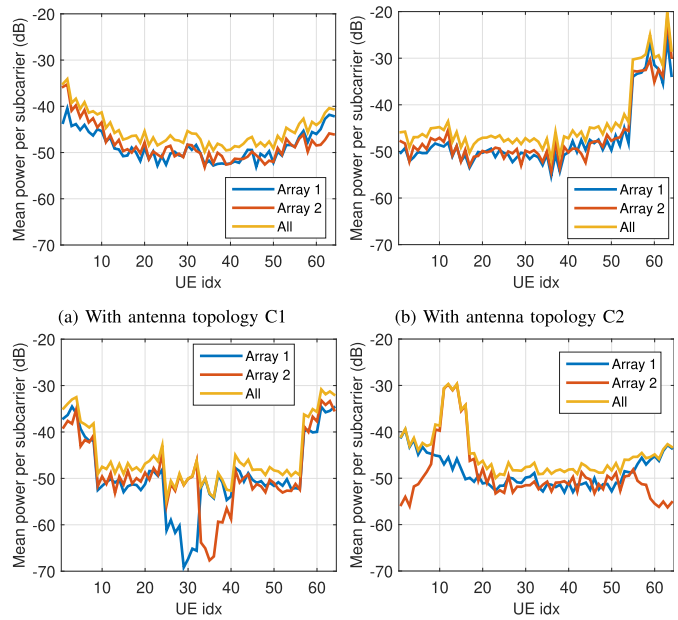

(a) With antenna topology C1

(b) With antenna topology C2

(c) With antenna topology D1

(d) With antenna topology D2

Fig. 5. The gain variation of each UE with four different antenna topologies.

four UEs at each time instant. As represented by the arrow, the two USRPs are moved step-wise towards the end of the table opposite to the antenna array and turned around towards the array for a total of 16 locations to emulate 64 UEs.

At each UE location, a total of 80 OFDM uplink pilot symbols are collected with a collection period of 100 ms. The LTE-like radio frame structure with a frequency-division multiplexing of the pilot symbols is designed, where each UE occupies 100 subcarriers with a 12-subcarrier spacing. The sampling rate is 30.72 MHz and the system runs at 2.61 GHz.

Measurement results. An overview of the averaged channel gain per UE as defined in Eq. (7) is presented. Fig. 5 demonstrates the gain variation of the UEs in the four scenarios. The BS does not receive the same power from all UEs [4] in any of the scenarios. Notably, the received

[4]Even if we arrange the array in the center of the table, due to the directivity of the array, the asymmetry in the receive signal strength cannot be alleviated. Similar situations are to other kinds of array. For instance, array composed of dipole antennas exhibit also array directivity [19]; Antennas in cylindrical array do not contribute equally towards any single direction.

power from the two antenna arrays A1 and A2 are plotted separately, for comparison. The gain distribution shows the following two main features: *array near-far effect* and *array directivity*.

1) *Near-far effect:* In this feature, UEs closer to the array benefit from higher desired signal strength. In the co-located topologies, two arrays receive a similar power level from the UEs; while in the distributed topologies, there is a gain imbalance between the two arrays. In short, the CSI in some UE positions of the distributed antenna topologies has higher weighting from one of the arrays. This can greatly reduce the IUC if two UEs have different weighting on the two arrays.
2) *Array directivity:* In this feature, the direction of the array's main beam contributes even more than the distance. For example, Fig. 5b reveals that UEs with indices 56-64 receive approximately 15 dB higher power than their neighbors. The cross-reference to our measured array pattern in an anechoic chamber shown in Fig. 9 of [19] indicates that the gain difference between the main beam and the side lobes is more than 12 dB. Fig. 5b shows a higher deviation, which can be explained by an extra contribution from the environment reflection.

VIII. Performance Evaluation

We first collect the channel measurement as introduced in Sec. VII. Then, we store it into a database, which has been made open to our community [9]. Therefore, the communication society can verify our algorithm or design their own algorithms [32]. In this section, our proposed algorithm is evaluated by matlab simulations relying on the measured channel data. Simulation parameters are listed in Table IV. The average sum-rate in each scenario is numerically evaluated by summing the averaged throughput of the UEs over 1000 scheduling slots. After each scheduling slot, the averaged historical spectral efficiency is updated, affecting the first UE being selected in the next scheduling slot. The signal-to-noise ratio (SNR) of the simulation refers to the average single antenna SNR as perceived by a single UE with the maximum received power in that scenario, SNR $\triangleq \frac{\max(\mathbb{E}(\bar{\mathbf{h}}_k))}{M\sigma_{UL}^2}$. Note that in a per-scenario basis, the same noise variance is applied to all the UEs.

We compare our proposed heuristic with two benchmarks.

- *Random scheduling:* in each scheduling slot, the BS randomly chooses K out of the S UEs to serve.
- *Capacity based scheduling:* The proposed method in [33] directly calculates the summation of capacity in each i_{th} iteration which involves calculation of Eqs. (5) and (6). The goal is to maximize the network SE at each iteration i when selecting a new UE (cf. Line 6 of Algorithm 1)

$$\delta_i = \left(\sum_{j=1}^{i-1} \mathrm{SE}_j + \mathrm{SE}_k \right). \tag{17}$$

Note that in each iteration, $\mathrm{SE}_j, \forall j \in \{1, \ldots, i\}$ should be recalculated, as they are mutually related. The advantage of this method is that it approaches to optimum.

TABLE IV
System Parameter Settings in the Evaluation

P_{max}	0 dBm
SNR	20 dB (averaged single antenna SNR of max power UE in each scenario)
OFDM symbol duration	71.4 μs
Scheduling slots	1000
Number of subcarriers	100
Number of OFDM symbols collected	80
K	2:2:64
S	64
M	64
Antenna topologies	C1, C2, D1 and D2

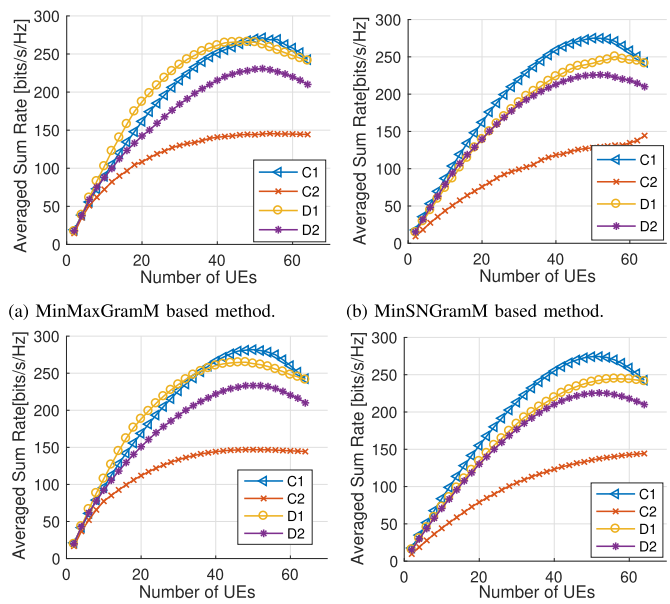

(a) MinMaxGramM based method. (b) MinSNGramM based method.

(c) Capacity based method. (d) Random selection based method.

Fig. 6. Averaged sum-rate vs. different number of selected UEs when there is no power control.

A. Performance Versus the Number of Served UEs

We first investigate the network performance versus the number of served UEs. Fig. 6 shows the results where the number of UEs served in each scheduling slot changes from 2 to 64 with a step of 2. The four investigated methods are labeled as "MinMaxGramM", "MinSNGramM", "Capacity" and "Random", respectively. We can clearly see that the performance of our proposed lightweight MinMaxGramM approaches to that of the Capacity based scheduling. An interesting observation from the results is the maximal number of UEs that the BS should serve (denoted as K^{opt}) when the network sum-rate reaches the maximum. For better visualization, we summarize in Table V the optimal K^{opt} and the corresponding achieved peak averaged sum-rate. We can notice that a method is superior if it reaches a peak with a lower number of K^{opt}.

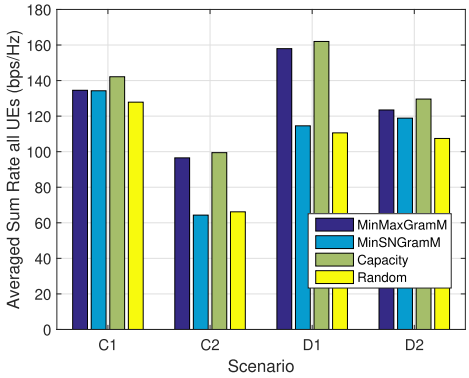

(a) Uplink averaged sum-rate

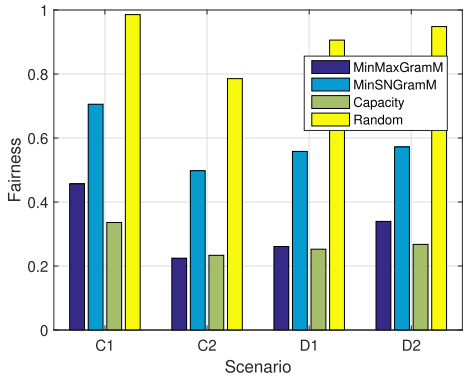

(b) Uplink user fairness

Fig. 7. Performance comparison of the uplink sum-rate under different antenna topologies *(without loss of generality, in the rest of this section we only show the results under the antenna topologies C1 and D1 in most of cases, due to the space limitations).*

Regarding the impact of the antenna topologies on the system performance, we can observe that the corresponding distributed antenna topology in scenario D1 performs the best than other antenna topologies. With this antenna topology, a reasonably low number of K UEs is selected.

In the rest of our simulations, we use $K = 16$. There are mainly two reasons for this choice: *1)* in a practical implementation of the precoder and receiver detector in massive MIMO networks, a $K \times K$ matrix inversion is required on a per subcarrier basis. The complexity of matrix inversion increases proportional to K. Therefore, a large K will result in significant complexity, making the design not practical; *2)* the authors in [34] have shown that in their implementation, 22 UEs can be served simultaneously with a 128-antenna testbed. We have 64 antennas in our testbed. Thus, we choose $K = 16$ to make our system more practical in a real network.

B. Performance Evaluation Without Power Control at the UEs

Next, we evaluate the performance of our heuristic scheduling algorithm, without considering power control at the UEs.

1) Sum-Rate: The averaged sum-rate comparison is presented in Fig. 7. We can observe from Fig. 7a that there is only 5% less different between our lightweight MinMaxGramM scheduling algorithm and the Capacity based scheduling. Remember that compared to the Capacity based algorithm, our MinMaxGramM can reduce the complexity by 99.5% as it is shown in Table I. With the antenna topologies C2 and D2,

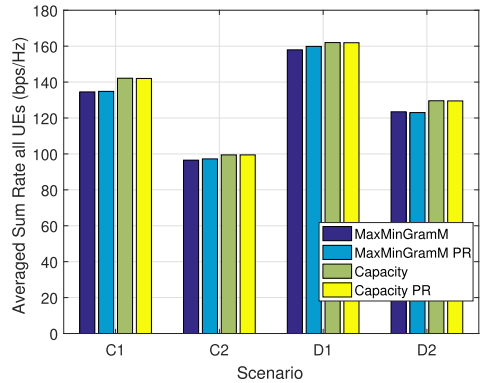

Fig. 8. Averaged sum-rate under our method for pilot overhead reduction.

we notice a big gap between the Capacity based and the Random scheduling algorithms. This gap indicates that a proper scheduling algorithm can improve spectral efficiency significantly under different antenna topologies of a massive MIMO network.

When studying the impact of antenna topologies on the performance of scheduling algorithms, we see clearly that antenna topology D1 benefits the Capacity based scheduling algorithm. With antenna topology C1, the performance of all the algorithms are quite similar, indicating that a carefully designed scheduling algorithm could be not needed. Low-complexity algorithms, such as the Random scheduling method, already performs quite well.

From Fig. 7b, we can clearly see a trade-off between sum-rate and user fairness. Taking the the Random scheduling algorithm for an example. The user fairness with antenna topology C2 and D1 is only around 0.2. This implied that for some co-scheduled UEs, their SINR degrade significantly due to IUC. In general, antenna topology C2 leads to the best user fairness performance.

2) Pilot Overhead Reduction: The pre-log factor $\frac{\tau_{ud}}{\tau_c}$ in Eq. (6) is influenced by the pilot overhead. This factor impacts the spectral efficiency. In our channel measurements with the testbed, every four UEs send the pilot sequences within the same *frequency resource block*, which is defined as 12 consecutive subcarriers. To obtain the channel superset of S UEs with the traditional pilot overhead, $\frac{S}{4}$ OFDM symbols, which occupy 1.14 ms, are needed. With our proposed pilot overhead reduction method, only $1 + \frac{K}{4}$ OFDM symbols are needed. That is equivalent to 0.36 ms. As a result, the pilot overhead is reduced by $1.14/0.36 = 3.2$ times in our method.

Next, we verify the performance loss of our proposed method. For the proposed pilot reduction method, we sequentially choose pilots from every four UEs in one frequency resource block, until we obtain the channel superset, the full CSI from all from all 64 UEs. Without loss of generality, we compare the performance of the Capacity based algorithm and our proposed MaxMinGramM for both the traditional and the proposed pilot overhead reduction method. The results are shown in Fig. 8. The PR in the legend stands for pilot overhead reduction. We clearly observe that there is no big difference on the sum-rate between our proposed pilot overhead reduction and the traditional pilot scheme, under all the four antenna

TABLE V

K^{opt} AND THE PEAK AVERAGED SUM-RATE ACHIEVED UNDER FOUR DIFFERENT ANTENNA TOPOLOGIES

	Number of K^{opt} UEs				Peak Average Sum-rate [bits/s/Hz]			
	MinMaxGramM	MinSNGramM	Capacity	Random	MinMaxGramM	MinSNGramM	Capacity	Random
C1	52	50	50	52	271	275	282	274
C2	54	64	48	64	146	144	147	144
D1	46	56	48	56	266	250	265	245
D2	52	52	50	52	231	226	233	226

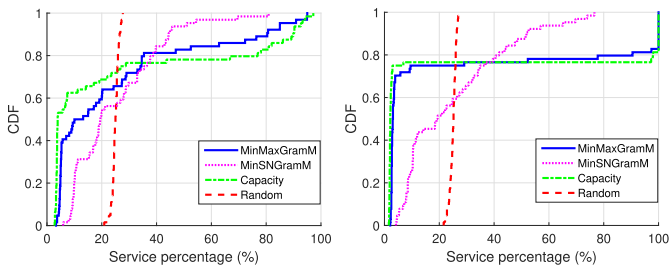

(a) With antenna topology C1 (b) With antenna topology D1

Fig. 9. Comparison of the uplink service percentage. The close to optimum solution in C1 and D1 is in favor of a small group of UEs which benefits simultaneously from higher power and lower IUC.

topologies. However, our proposed method can reduce the pilot overhead significantly as presented in the previous paragraph.

3) UE Served Percentage: The results are given in Fig. 9. With the Random scheduling algorithm, the mean served rate is close to 25%, as expected (16/64). For the Capacity based scheduling, we notice that it under-serves about 70% of UEs. With our proposed MinMaxGramM and MinSNGrmM, this majority of UEs are served with much probability because in *Step 1* of our heuristic (cf. Sec. IV), we give the highest priority to the UE that is least served. Another interesting observation can be seen from Fig. 9b: with antenna topology of D1, around 20% of UEs are served 100% of the time. The reason behind this phenomenon is that these UEs have a very good channel quality. Our proposed heuristic tends to selected a group of UEs which have both low IUC and high received power at the BS.

To gain more insights on why some UEs are selected under a certain scheduling algorithm, we plot the received power map and UEs' served probability map under the Capacity based scheduling algorithm, without loss of generality. The results are shown in Fig. 10 and Fig. 11. The UEs located in the extreme high power region under antenna topology D1 have a higher probability to be served. This can be explained by the corresponding deployment of the antennas: with D1, and only a few UEs are covered by the main beam while the majority of the UEs are in the side lobes. The main beam guarantees not only a high received power from the UEs but also low IUC among the UEs. This topology benefits a small group of UEs that are within the coverage of the main beam. As a comparison, with the antenna topology C1, the two arrays are located in the front of the room. Therefore, almost all the UEs are covered by the main beam. From the user selection probability map given in Fig. 11a, we can see that the UEs are served more balanced with the antenna topology C1.

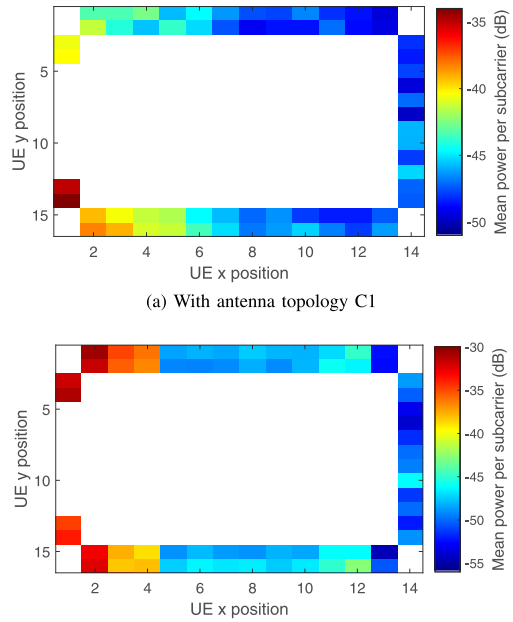

(a) With antenna topology C1

(b) With antenna topology D1

Fig. 10. Received power map vs. UEs' locations. Each small grid in the map denotes the BS's received power from each UE.

4) Improving the User Fairness: We further investigate if we can improve the user fairness performance while not sacrificing too much the max sum-rate. Without the loss of the generality, we focus on the proposed MinMaxGramM method. In Fig. 12, the number of prioritized UEs K_{pri} is changed from 1 to 8. For C1, the user fairness can reach almost one when the number of prioritized users reaches seven. However, the performance also drops to that of Random selection. For D1, the ideal number of prioritized users should be five, especially if we want to keep the performance of D1 higher than that of C1; in this case, the user fairness approaches 0.5. By looking at the served percentage with cumulative distribution function (CDF) in Fig. 13, it can be further confirmed that with the adoption of K_{pri} in our heuristic scheduling, the majority of UEs can get at least 10% of data service in all scenarios.

C. Performance Evaluation With Power Control

As big power imbalance between the UEs is observed in Fig. 5 and 10. With antenna topology D1, the range of the received power spanned more than 25 dB while for antenna topology C1, the range is 20 dB. In this section, we study the impact of power control on the user fairness.

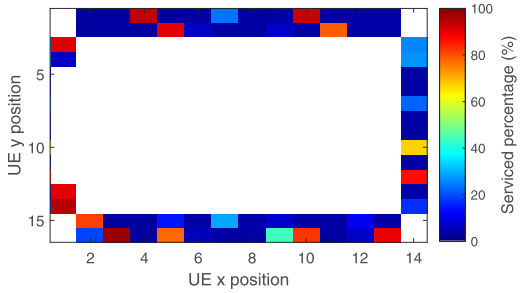

(a) With antenna topology C1

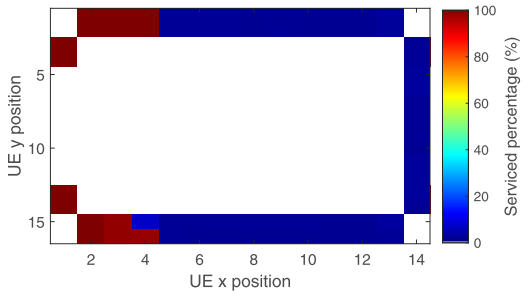

(b) With antenna topology D1

Fig. 11. Serving percentage per UE under the Capacity based scheduling algorithm vs. UEs' absolute locations. Each small grid in the map represents the served probability of a single UE.

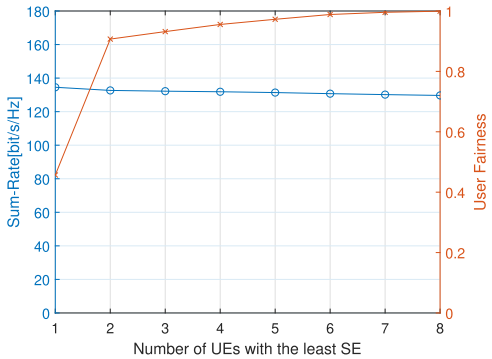

(a) With antenna topology C1

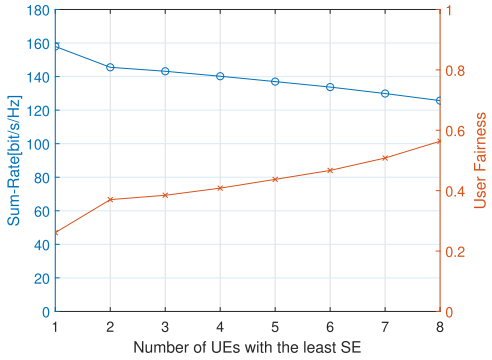

(b) With antenna topology D1

Fig. 12. Improvement of user fairness by the adoption of K_{pri} in our proposed heuristic scheduling.

In our system-level simulation, we apply power control to all UEs according to Eq. (16). The differentiated transmission power of each UE affects the input of Algorithm 1, as a result, leading to different sum-rate. The results are shown in Fig. 14. We only focus on MinMaxGramM as it approaches the upper bound obtained by the Capacity based scheduling.

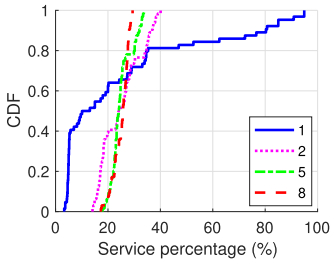

(a) With antenna topology C1

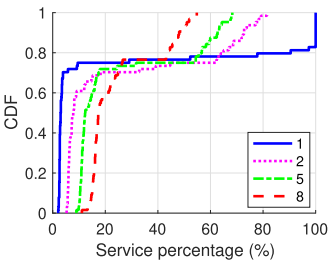

(b) With antenna topology D1

Fig. 13. Improvement of user fairness by the adoption of K_{pri} in our heuristic scheduling. The served CDF are compared when K_{pri} is set to 1, 2, 5 and 8.

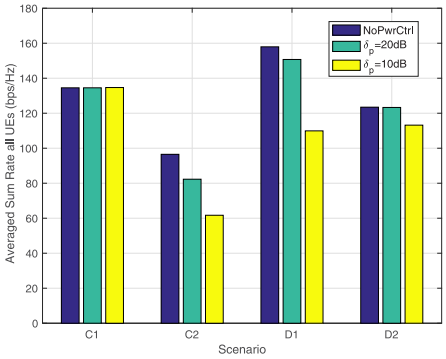

(a) Averaged sum-rate with power control

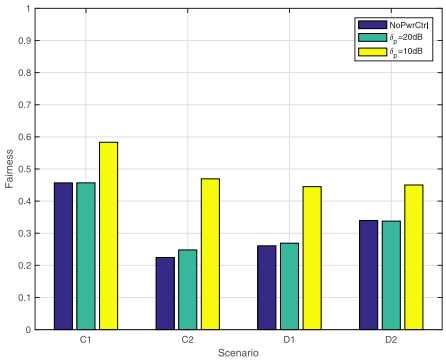

(b) User fairness with power control

Fig. 14. Comparison of the uplink averaged sum-rate for different levels of power control with our MinMaxGramM algorithm.

Two levels of power control, δ_p =20 dB and δ_p =10 dB, are investigated. The results are compared with the settings without power control. We can observe from Fig. 14a that with antenna topology D1, the sum-rate degrades significantly when the power delta limit δ_p equals 10 dB. This is because the received power imbalance is larger with this antenna topology. In Fig. 14b, we can notice that the user fairness benefits from limiting the power imbalance δ_p to 10 dB.

To gain more insights on how the UEs are scheduling, we present the UEs' served percentage in Fig. 15, under our proposed MinMaxGramM algorithm. When δ_p equals 20 dB, there is no big change in the served probability distribution, especially with antenna topology C1. In contrast, MinMaxGramM treats UEs more equally when δ_p equals 10 dB. However, there are still about 40% of the UEs suffer from unequal data service. Finally, we compare all

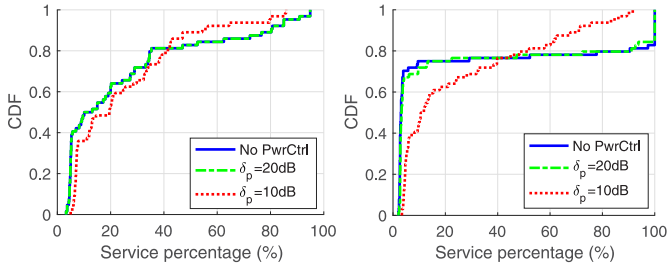

(a) With antenna topology C1 (b) With antenna topology D1

Fig. 15. Comparison of the uplink served percentage for different levels of power control with our MinMaxGramM algorithm.

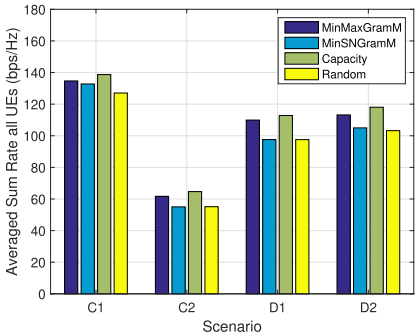

(a) Average sum-rate with power control

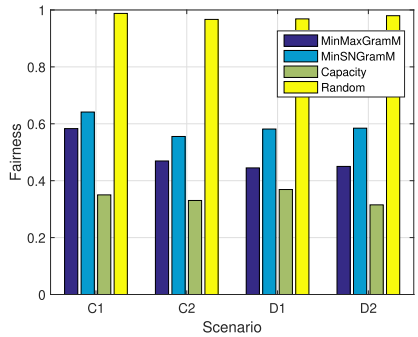

(b) User fairness with power control

Fig. 16. Comparison of the uplink averaged sum-rate with power control $\delta_p = 10$ dB at the UEs.

the scheduling algorithm with power control. The results are shown in Fig. 16. Regarding the sum-rate, our MinMaxGramM still performs very close to the Capacity based scheduling algorithm. However, with antenna topology D1 the user fairness under MinMaxGramM is above 0.45 for all scenarios, better than the Capacity based scheduling algorithm. To sum up, using power control does not improve significantly the user fairness. On the contrary, the system throughput drops due to the lowered overall transmission power.

IX. Conclusion

In this paper, we tackled an issue rising in the massive MIMO empowered dense networks: system performance degradation due to the high inter-user correlation of closely located UEs. We designed a low-complexity scheduling algorithm that can accurately select high power UEs with relatively low correlation. With four different antenna topologies, we evaluated the performance of our proposed algorithm. Our results showed that the proposed heuristic algorithm performed strictly to the sub-optimal but very complicated Capacity based approach. To improve the user fairness, we further proposed a priority based method that obtained user fairness of more than 0.5 with all the considered antenna topologies. We envision that our study will give insights for the deployment of future indoor applications which support multiple user scheduling empowered massive MIMO networks.

References

[1] C.-M. Chen, Q. Wang, A. Gaber, A. P. Guevara, and S. Pollin, "Experimental study of user selection for dense indoor massive MIMO," in *Proc. IEEE INFOCOM Conf. Comput. Commun. Workshops (INFOCOM WKSHPS)*, Apr. 2019, pp. 1–6.

[2] T. L. Marzetta, "Noncooperative cellular wireless with unlimited numbers of base station antennas," *IEEE Trans. Wireless Commun.*, vol. 9, no. 11, pp. 3590–3600, Nov. 2010.

[3] E. Björnson, J. Hoydis, and L. Sanguinetti, "Massive MIMO networks: Spectral, energy, and hardware efficiency," *Found. Trends Signal Process.*, vol. 11, nos. 3–4, pp. 154–655, 2017.

[4] C.-M. Chen, V. Volskiy, A. Chiumento, L. Van der Perre, G. A. E. Vandenbosch, and S. Pollin, "Exploration of user separation capabilities by distributed large antenna arrays," in *Proc. IEEE Globecom Workshops (GC Wkshps)*, Dec. 2016.

[5] H. Yang and T. L. Marzetta, "Massive MIMO with max-min power control in Line-of-Sight propagation environment," *IEEE Trans. Commun.*, vol. 65, no. 11, pp. 4685–4693, Nov. 2017.

[6] H. Q. Ngo, E. G. Larsson, and T. L. Marzetta, "Aspects of favorable propagation in massive MIMO," in *Proc. Signal Process. Conf. (EUSIPCO)*, 2014, pp. 76–80.

[7] X. Gao, O. Edfors, F. Rusek, and F. Tufvesson, "Massive MIMO performance evaluation based on measured propagation data," *IEEE Trans. Wireless Commun.*, vol. 14, no. 7, pp. 3899–3911, Jul. 2015.

[8] C.-M. Chen, A. P. Guevara, and S. Pollin, "Pilot contamination in massive MIMO: A measurement-based analysis using 2D-MUSIC," in *Proc. IEEE Signal Process. Adv. Wireless Commun.*, 2018, pp. 1–5.

[9] *Massive MIMO Indoor Experiment Data Set*. Accessed: Oct. 3, 2019. [Online]. Available: https://github.com/networkedsystems/MaMIMO_indoor

[10] K. Wang and K. Psounis, "Scheduling and resource allocation in 802.11 ax," in *Proc. INFOCOM IEEE Conf. Comput. Commun.*, Apr. 2018, pp. 279–287.

[11] H. Yang and T. L. Marzetta, "Massive MIMO with max-min power control in line-of-sight propagation environment," *IEEE Trans. Commun.*, vol. 65, no. 11, pp. 4685–4693, Nov. 2017.

[12] H. Yang, "User scheduling in massive MIMO," in *Proc. IEEE 19th Int. Workshop Signal Process. Adv. Wireless Commun. (SPAWC)*, Jun. 2018, pp. 1–5.

[13] Y. Xu, G. Yue, and S. Mao, "User grouping for massive MIMO in FDD systems: New design methods and analysis," *IEEE Access*, vol. 2, pp. 947–959, 2014.

[14] G. Lee and Y. Sung, "Asymptotically optimal simple user scheduling for massive MIMO downlink with two-stage beamforming," in *Proc. IEEE 15th Int. Workshop Signal Process. Adv. Wireless Commun. (SPAWC)*, Jun. 2014, pp. 60–64.

[15] A. Adhikary, J. Nam, J. Ahn, and G. Caire, "Joint spatial division and multiplexing—The large-scale array regime," *IEEE Trans. Inf. Theory*, vol. 59, no. 10, pp. 6441–6463, Oct. 2013.

[16] J. Nam, A. Adhikary, J.-Y. Ahn, and G. Caire, "Joint spatial division and multiplexing: Opportunistic beamforming, user grouping and simplified downlink scheduling," *IEEE J. Sel. Topics Signal Process.*, vol. 8, no. 5, pp. 876–890, Oct. 2014.

[17] H. Liu, H. Gao, S. Yang, and T. Lv, "Low-complexity downlink user selection for massive MIMO systems," *IEEE Syst. J.*, vol. 11, no. 2, pp. 1072–1083, Jun. 2017.

[18] X. Gao, J. Flordelis, G. Dahman, F. Tufvesson, and O. Edfors, "Massive MIMO channel modeling—Extension of the COST 2100 model," in *Proc. Joint NEWCOM/COST Workshop Wireless Commun.(JNCW)*, vol. 1, Oct. 2015, pp. 4558–4563.

[19] C.-M. Chen, V. Volski, L. Van der Perre, G. Vandenbosch, and S. Pollin, "Finite large antenna arrays for massive MIMO: Characterization and system impact," *IEEE Trans. Antennas Propag.*, vol. 65, no. 12, pp. 6712–6720, Dec. 2017.

[20] B. Friedlander and A. Weiss, "Direction finding in the presence of mutual coupling," *IEEE Trans. Antennas Propag.*, vol. 39, no. 3, pp. 273–284, Mar. 1991.
[21] S. O. K. Zheng and X. Yin, "Massive MIMO channel models: A survey," *Int. J. Antennas Propag.*, vol. 2014, p. 10, Jun. 2014.
[22] Y. Jiang, M. K. Varanasi, and J. Li, "Performance analysis of ZF and MMSE equalizers for MIMO systems: An in-depth study of the high SNR regime," *IEEE Trans. Inf. Theory*, vol. 57, no. 4, pp. 2008–2026, Apr. 2011.
[23] X. Gao, O. Edfors, F. Rusek, and F. Tufvesson, "Linear pre-coding performance in measured very-large MIMO channels," in *Proc. VTC Fall*, 2011, pp. 1–5.
[24] R. K. Jain, D.-M. W. Chiu, and W. R. Hawe, "A quantitative measure of fairness and discrimination," *Eastern Res. Lab., Digit. Equip. Corp.*, Hudson, MA, USA, 1984.
[25] G. Dimic and N. D. Sidiropoulos, "On downlink beamforming with greedy user selection: Performance analysis and a simple new algorithm," *IEEE Trans. Signal Process.*, vol. 53, no. 10, pp. 3857–3868, Oct. 2005.
[26] D. Hammarwall, M. Bengtsson, and B. Ottersten, "Utilizing the spatial information provided by channel norm feedback in SDMA systems," *IEEE Trans. Signal Process.*, vol. 56, no. 7, pp. 3278–3293, Jul. 2008.
[27] *MIMO Prototyping System Getting Started Guide*. Accessed: Oct. 3, 2019. [Online]. Available: http://www.ni.com/pdf/manuals/376638b.pdf
[28] J. Vieira *et al.*, "A flexible 100-antenna testbed for massive MIMO," in *Proc. Globecom Workshops*, 2014.
[29] S. Payami and F. Tufvesson, "Channel measurements and analysis for very large array systems at 2.6 GHz," in *Proc. 6th Eur. Conf. Antennas Propag. (EUCAP)*, 2012, pp. 433–437.
[30] M. Gauger, J. Hoydis, C. Hoek, H. Schlesinger, A. Pascht, and S. ten Brink, "Channel measurements with different antenna array geometries for massive MIMO systems," in *Proc. ITG SCC*, 2015, pp. 1–6.
[31] C.-M. Chen *et al.*, "Distributed massive MIMO: A diversity combining method for TDD reciprocity calibration," in *Proc. GLOBECOM IEEE Global Commun. Conf.*, Dec. 2017, pp. 1–7.
[32] *Emil Björnson*. Accessed: Jan. 19, 2019. [Online]. Available: https://ma-mimo.ellintech.se/2019/01/19/dataset-with-channel-measurements-for-distributed-and-co-located-massive-mimo/
[33] Z. Shen, R. Chen, J. G. Andrews, R. W. Heath, and B. L. Evans, "Low complexity user selection algorithms for multiuser MIMO systems with block diagonalization," in *Proc. Conf. Rec. 39th Asilomar Conf. Signals, Syst. Comput.*, 2005, pp. 628–632.
[34] P. Harris *et al.*, "Serving 22 users in real-time with a 128-antenna massive MIMO testbed," in *Proc. IEEE Int. Workshop Signal Process. Syst. (SiPS)*, Oct. 2016, pp. 266–272.

Cheng-Ming Chen (Student Member, IEEE) received the M.S. degree from the Graduate Institute of Communication Engineering, National Taiwan University (NTU), Taipei, Taiwan, in 2006, and the Ph.D. degree in electrical engineering from KU Leuven, Belgium, in 2019, investigating distributed massive MIMO system with software-defined radio. From 2006 to 2011, he has worked on the baseband design of WiMAX and LTE with the Industrial Technology of Research Institute (ITRI), Hsinchu. He was involved in the 802.16m standardization at ITRI. From 2011 to 2015, he was with Broadcom as a Senior System Design Engineer, mainly focused on WiFi receiver bringup. Since 2019, he has been a WiFi Algorithm Design Senior Staff Engineer with Qualcomm.

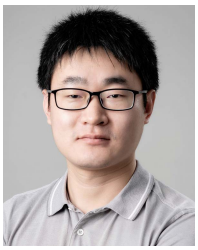

Qing Wang (Member, IEEE) received the B.E. and M.S. degrees from the University of Electronic Science and Technology of China, in 2008 and 2011, respectively, the M.S. degree from the IMDEA Networks Institute in 2012, and the Ph.D. degree from the University Carlos III of Madrid in 2016. He was an FWO Post-Doctoral with KU Leuven, Belgium. He is an Assistant Professor with the Department of Software Technology, Delft University of Technology (TU Delft), The Netherlands. His research interests include beyond 5G networking, visible light communication, and the Internet of Things.

Abdo Gaber (Member, IEEE) was born in Sana'a, Yemen. He received the B.Sc. degree in electronics and communications from Sana'a University, Yemen, in 2005, and the M.Sc. and Dr.-Ing. degrees in wireless communications with a grant from the DAAD from the University of Jordan, Jordan, and the University of Magdeburg, Germany, in 2009 and 2015, respectively. He was a BSS Engineer with Sabafon Communication Company from 2005 to 2006 and a Microwave Transmission Supervisor with MTN Communication Company from 2009 to 2010. He was a Researcher with the University of Magdeburg from 2014 and 2016. He is currently working with National Instruments Dresden on advanced wireless research. His main research interest includes wireless communication systems.

Andrea P. Guevara (Student Member, IEEE) received the B.Sc. degree in electronics and telecommunications from the University of Cuenca, Ecuador, in 2013, and the M.Sc. degree in telecommunications by research from the Faculty of Natural and Mathematical Sciences, King's College London, U.K., in 2015. She is currently pursuing the Ph.D. degree with KU Leuven. She worked as a Telecommunications Consultant in spectrum regulation. She received the prize for the Best Academic Performance on the M.Sc. by Research Programme from the Faculty of Natural and Mathematical Sciences, King's College London. Her main research interests include massive MIMO, infrastructure sharing, and inter-cell interference.

Sofie Pollin (Senior Member, IEEE) received the Ph.D. degree (Hons.) from KU Leuven in 2006. From 2006 to 2008, she continued her research on wireless communication, energy-efficient networks, cross-layer design, coexistence, and cognitive radio at UC Berkeley. In November 2008, she returned to imec to become a Principal Scientist with the Green Radio Team. She is currently an Associate Professor with the Electrical Engineering Department, KU Leuven. Her research interests include networked systems that require networks that are ever denser, heterogeneous, battery powered, and spectrum constrained. She is a BAEF and a Marie Curie Fellow.